Investigations of the Thermal Response of Laser-Excited Biomolecules

P. Li and P. M. Champion
Department of Physics, Northeastern University, Boston, MA 02115

ABSTRACT A model is presented that connects the underlying classical thermal transport coefficients to the experimentally determined vibrational temperature of a photoexcited chromophore embedded in a protein matrix that is surrounded by water. Both photostationary state heating (e.g., within a 10-ns laser pulse) and transient cooling (e.g., after termination of the laser pulse) are treated. Because only a few thermal transport parameters can be experimentally determined, this simple model provides a practical and efficient method for describing the temperatures of the chromophore, protein, and solvent as functions of time and position. We expect that such a model will be useful in interfacing experimental observations with more elaborate molecular dynamics calculations, which depend upon many variables. In the transient cooling process, which is relevant for ultrafast pulsed laser measurements, the temperature of the chromophore follows a double exponential decay at short times, whereas at longer times the thermal decay "rolls over" to a diffusion limit ($t^{-3/2}$). For typical 10-ns laser pulses (~ 0.5 GW/cm^2) and chromophore absorption cross-sections ($\sim 10^{-16}$ cm^2), we find that the biomolecule reaches thermal steady-state on a ps time scale. The role of the various thermal transport coefficients and their independent experimental determination is also discussed.

INTRODUCTION

In chromophoric biomolecules such as heme proteins, rhodopsins, or photsynthetic reaction centers, the photon energy absorbed by the chromophore is rapidly converted to heat (vibrational energy) causing the temperature of the chromophore to increase. For example, time-resolved anti-Stokes resonance Raman spectra of heme proteins (Lingle et al., 1991a,b; Li et al., 1992) and bacteriorhodopsin (Brack and Atkinson, 1991) have shown that the vibrational temperature of the chromophore is significantly increased after absorption of photons. Ultrafast laser pulses are now being used routinely to measure biologically relevant kinetic processes. However, during the measurement the chromophore can potentially become very hot (Henry et al., 1986) (for cytochrome c, the heat capacity of the heme group is about $10^{-21}J/K$ and excitation at $\lambda_L = 420\ nm$ leads to $\Delta T \sim 5\times 10^2 K$/photon, if all the excitation energy is localized in the heme ground state vibrational manifold). As a result, the time scale for the dissipation of excess vibrational energy must be considered in analyzing the kinetics of photon-driven biological processes. In this work, we analyze heating and cooling processes in photo-excited biomolecules and use the resulting temperature profile of the chromophore to assess the time scale over which the photoexcitation can affect the biological rates.

Two basic approaches that can be used to study energy dissipation in biomolecules are molecular dynamics simulations (Henry et al., 1986) and classical heat transport calculations (Kesavamoorthy et al., 1992; Li et al., 1992; Carslaw and Jaeger, 1959). One disadvantage of the molecular dynamics simulations is the difficulty of connecting the many internal parameters to the experimental measurements. In the classical heat transport model presented here, only a few thermal parameters are needed, and many of them can be determined by independent experimental measurements.

A previous one boundary thermal transport model was used by Asher and co-workers to simulate photothermal dynamics in colloidal particles suspended in water (Kesavamoorthy et al., 1992). However, there seems to be a problem in the application of this model.[1] In the present work, a classical two boundary thermal transport model is developed to simulate the thermal dynamics of both photo-stationary heating and transient cooling in chromophoric biomolecules.

THEORY

One boundary model

We first consider the thermal response of a perfectly conducting sphere[2] with heat capacity C_h and radius a, surrounded by solvent with density ρ, specific heat c, thermal conductivity K, and surface conductivity H. The heat transfer will be governed by (Carslaw and Jaeger, 1959)

$$K\frac{\partial^2(rT)}{\partial r^2} - \rho c\frac{\partial(rT)}{\partial t} = 0; \qquad (1)$$

Received for publication 19 August 1993 and in final form 22 November 1993.

Address reprint requests to Dr. Paul M. Champion, Dept. of Physics, Northeastern University, 360 Huntington Ave., Boston, MA 02115.

0006-3495/94/02/430/07 $2.00

[1] A version of Newton's law of cooling, which assumes perfect thermal conduction inside the particle, was applied by Kesavamoorthy et al., 1992. Yet, their solutions show a spatial variation of temperature within the particle (Fig. 4, Kesavamoorthy et al., 1992) that is inconsistent with this assumption. Similarly, the time evolution of the temperature profiles depict (Fig. 1, Kesavamoorthy et al., 1992) a period (10–100 ns) during which the water temperature at the surface of the particle exceeds that of the particle surface itself. Continued cooling would therefore require that heat flow from a cooler to a hotter surface element, in violation of the second law of thermodynamics.

[2] The assumption of perfect conductivity corresponds to rapid intramolecular vibrational redistribution, which has been previously established for large chromophores (Miller, 1991).

with the boundary conditions:

$$C_h \frac{\partial T_h}{\partial t} + 4\pi a^2 H(T_h - T) = \dot{Q}, \quad \text{for} \quad r = a;$$
$$K \frac{\partial T}{\partial r} + H(T_h - T) = 0, \quad \text{for} \quad r = a, \tag{2}$$

where $\dot{Q}$ is the rate of heat absorption of the chromophore because of photon excitation, T_h is the temperature of the chromophore, and the T is the temperature of the surrounding solvent. For convenience, we will assume that the rate of heat absorption is both constant and continuous in time. Obviously, these assumptions are correct for the transient cooling process ($\dot{Q} = 0$), but when $\dot{Q} \neq 0$ heat absorption will not be continuous on very short (~ps) time scales. In addition, ground state population bleaching (Li et al., 1992) and the temperature dependence of the optical absorption lineshape (Schomacker and Champion, 1986) both lead to a time dependence in the rate of heat absorption of the chromophore. Here we take $\dot{Q}$ as a constant corrected for saturation (bleaching) effects (Li et al., 1992) and consider the heat absorption on short time scales using an average value for $\langle \dot{Q} \rangle$, inasmuch as the experiment interrogates many molecules in the laser beam region.

We assume initial conditions of $T_h = T^*$ and $T = T_0$ at $t = 0$. If we let $T_0 = 0$ (*i.e.*, re-scale temperature T_0 to zero) and do the Laplace transformation, Eq. 1 and Eq. 2 will become

$$\frac{d^2(r\bar{T})}{dr^2} - \frac{p}{\kappa}(r\bar{T}) = 0; \tag{3}$$

and

$$C_h(p\bar{T}_h - 1) + 4\pi a^2 H(\bar{T}_h - \bar{T}) = \frac{\langle \dot{Q} \rangle}{p}, \quad \text{for} \quad r = a;$$
$$\frac{d\bar{T}}{dr} + h(\bar{T}_h - \bar{T}) = 0, \quad \text{for} \quad r = a. \tag{4}$$

Where p is the Laplace transform parameter, $\kappa = K/\rho c$ and $h = H/K$.

So long as $\bar{T}$ has a finite value when $r \to \infty$, Eq. 3 leads to

$$\bar{T} = \frac{A}{r} e^{-\sqrt{(p/\kappa)}r}$$
$$\frac{d\bar{T}}{dr} = -\frac{1 + r\sqrt{p/\kappa}}{r^2} A e^{-\sqrt{(p/\kappa)}r}. \tag{5}$$

Putting the expressions for $\bar{T}$ and $d\bar{T}/dr$ into Eq. 4 gives

$$\bar{T}_h = \frac{a^2(pC_hT^* + \langle \dot{Q} \rangle)(1 + ah + a\sqrt{p/\kappa})}{C_h p\kappa[(a\sqrt{p/\kappa})^3 + (a\sqrt{p/\kappa})^2(1 + ah) + Dah(1 + a\sqrt{p/\kappa})]},$$
$$\bar{T} = \frac{a^4(pC_hT^* + \langle \dot{Q} \rangle)e^{-\sqrt{(p/\kappa)}(r-a)}}{rpC_h\kappa[(a\sqrt{p/\kappa})^3 + (a\sqrt{p/\kappa})^2(1 + ah) + Dah(1 + a\sqrt{p/\kappa})]}. \tag{6}$$

where $D = 4\pi a^3 \rho c/C_h$.

In the case of $T^* \neq 0$ and $\langle \dot{Q} \rangle = 0$, Eq. 6 gives the thermal cooling profile after short pulse excitation. Using the inverse Laplace transform (see APPENDIX), we find

$$T_h = \frac{2a^2 DT^* h^2}{\pi} \cdot \int_0^\infty \frac{e^{-\kappa u^2 t/a^2} u^2 \, du}{[u^2(1 + ah) - Dah]^2 + (u^3 - Dahu)^2} \tag{7}$$

For small times or large values of K/H, Eq. 7 is approximated by

$$T_h = T^* e^{-t/\tau_c} \tag{8}$$

with a cooling time constant $\tau_c = a/Dh\kappa = C_h/4\pi a^2 H$.

At long times Eq. 7 goes as

$$T_h = \frac{T^* a^3}{2D\pi^{1/2}(\kappa t)^{3/2}} + \frac{3T^* a^4[2 + ah(2 - D)]}{4hD^2\pi^{1/2}(\kappa t)^{5/2}} + \cdots, \tag{9}$$

where the first term can be identified as the thermal diffusion limit.

In the case of $T^* = 0$ and $\langle \dot{Q} \rangle \neq 0$, Eq. 6 describes the process of chromophore heating by photon absorption. Using the inverse Laplace transform,

$$T_h = \frac{\langle \dot{Q} \rangle}{4\pi aK} \left\{ \frac{1 + ah}{ah} - \frac{2a^2 D^2 h^2}{\pi} \cdot \int_0^\infty \frac{e^{-\kappa u^2 t/a^2} \, du}{[u^2(1 + ah) - Dah]^2 + [u^3 - Dahu]^2} \right\}, \tag{10}$$

we find

$$T_h = \frac{\langle \dot{Q} \rangle}{C_h} \left[t - \frac{Dh\kappa t^2}{2a} + \cdots \right], \tag{11}$$

for small value of the time, and

$$T_h = \frac{\langle \dot{Q} \rangle}{4\pi Ka} \left\{ \frac{1 + ah}{ah} - \frac{a}{(\pi\kappa t)^{1/2}} - \frac{a^2[2 + ah(2 - D)]}{2hD\pi^{1/2}(\kappa t)^{3/2}} + \cdots \right\}, \tag{12}$$

for $t \to \infty$. The first term in Eq. 12 gives the temperature when photostationary state conditions are achieved (e.g., within a 10-ns laser pulse).

Two boundary model

To more accurately describe heat dissipation in chromophoric biomolecules, we develop a two boundary model (Fig.1) having a perfectly conducting core (chromophore) covered by a shell of protein material that is surrounded by solvent. Here we take K_1 and K_2 to describe the thermal conductivities of the protein and the surrounding solvent. The surface conductivities for the chromophore/protein and protein/solvent boundaries are given by H_1 and H_2 respectively, and C_h is the heat capacity of the chromophore. The quantities c_1 and c_2, ρ_1 and ρ_2 are the specific heats,

and densities of the protein and solvent, whereas T_h, T_1 and T_2 describe the temperatures of chromophore, protein and solvent.

The heat transfer in this model is determined by

$$K_1 \frac{\partial^2(rT_1)}{\partial r^2} - \rho_1 c_1 \frac{\partial(rT_1)}{\partial t} = 0;$$
$$K_2 \frac{\partial^2(rT_2)}{\partial r^2} - \rho_2 c_2 \frac{\partial(rT_2)}{\partial t} = 0; \tag{13}$$

with the boundary conditions (Fig. 1):

$$C_h \frac{\partial T_h}{\partial t} + 4\pi a_1^2 H_1 (T_h - T_1) = \langle \dot{Q} \rangle, \qquad \text{for} \quad r = a_1;$$
$$K_1 \frac{\partial T_1}{\partial r} + H_1 (T_h - T_1) = 0, \qquad \text{for} \quad r = a_1;$$
$$K_2 \frac{\partial T_2}{\partial r} + H_2 (T_1 - T_2) = 0, \qquad \text{for} \quad r = a_2; \tag{14}$$
$$K_1 \frac{\partial T_1}{\partial r} = K_2 \frac{\partial T_2}{\partial r}, \qquad \text{for} \quad r = a_2.$$

Using the initial conditions of $T_h = T^*$ and $T_1 = T_2 = T_0 = 0$ at $t = 0$ (when the laser pulse switches on, we take $T^* = 0$ and $\langle \dot{Q} \rangle \neq 0$; when the laser pulse switches off, we take $T^* \neq 0$ and $\langle \dot{Q} \rangle = 0$), we perform a Laplace transform on Eqs. (13) and (14) to find

$$\bar{T}_h(\sqrt{p}) = \frac{(T^* p + \langle \dot{Q} \rangle / C_h)\,[f_2 G_1 e^{-R_1\sqrt{p}} + f_5 G_2 e^{-R(2a_2/a_1 - 1)\sqrt{p}}]}{L(\sqrt{p})};$$
$$\bar{T}_1(\sqrt{p}) = \frac{a_1 S_1 (T^* p + \langle \dot{Q} \rangle / C_h)[G_1 e^{-R_1(r/a_1)\sqrt{p}} + G_2 e^{-R_1[(2a_2 - r)/a_1]\sqrt{p}}]}{rL(\sqrt{p})}; \tag{15}$$
$$\bar{T}_2(\sqrt{p}) = \frac{2a_2 S_1 S_2 K_1 R_1 \sqrt{p}(T^* p + \langle \dot{Q} \rangle / C_h) e^{-[(a_2/a_1)R_1 + ((r - a_2)/a_2)R_2])\sqrt{p}}}{rL(\sqrt{p})}.$$

with

$$L(\sqrt{p}) = (Ff_2 - a_1 S_1 D) G_1(\sqrt{p}) p e^{-R_1\sqrt{p}} + (Ff_5 - a_1 S_1 D) G_2(\sqrt{p}) p e^{-R_1[(2a_2/a_1) - 1]\sqrt{p}}, \tag{16}$$

and

$$G_1 = K_1(1 + S_2 + R_2\sqrt{p})\left(\frac{a_2}{a_1} R_1 \sqrt{p} - 1\right) + S_2 K_2 (1 + R_2\sqrt{p});$$
$$G_2 = K_1(1 + S_2 + R_2\sqrt{p})\left(1 + \frac{a_2}{a_1} R_1 \sqrt{p}\right) - S_2 K_2 (1 + R_2\sqrt{p}); \tag{17}$$

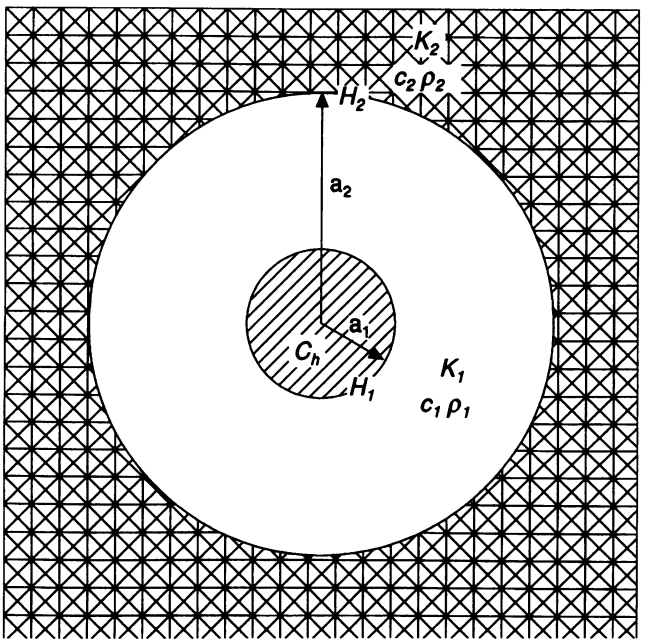

FIGURE 1 The two boundary classical heat transport model for a solvated biomolecule of radius a_2 with an embedded chromophore of radius a_1.

where

$$F = a_1 D + p,$$
$$f_2 = 1 + S_1 + R_1\sqrt{p}, \tag{18}$$
$$f_5 = 1 + S_1 - R_1\sqrt{p};$$

and $R_1 = a_1\sqrt{c_1\rho_1/K_1}$, $R_2 = a_2\sqrt{c_2\rho_2/K_2}$, $S_1 = a_1 h_1$, $S_2 = a_2 h_2$, $D = 4\pi a_1 H_1 / C_h$.

To get T_h, T_1 and T_2, we can use the inverse Laplace transform and do a numerical calculation (see Appendix)

$$T_j = \lim_{p \to 0} p\bar{T}_j(p) + \frac{1}{\pi}\int_0^{+\infty} \mathrm{Im}[\bar{T}_j(-i\sqrt{p})] e^{-pt}\, dp, \qquad (j = h, 1, 2). \tag{19}$$

For small values of time or large K_1/H_1, K_2/H_2 with small $R_c = 3C_h/4\pi a_1^3 \rho_1 c_1$ (for heme proteins, $R_c \leq 0.05$), the chromophore cooling can be described as a double exponential decay

$$T_h \sim (1 - A)e^{-k_1 t} + Ae^{-k_2 t}; \tag{20}$$

where

$$A = \frac{k_1 - k_{c1}}{k_1 - k_2},$$
$$k_1 = (1 + R_c)k_{c1} - \frac{R_c k_{c1} k_{c2}}{k_{c2} - (1 + R_c)k_{c2}},$$

and

$$k_2 = k_{c2} + \frac{R_c k_{c1} k_{c2}}{k_{c2} - (1 + R_c)k_{c1}},$$

with

$$k_{c1} = \frac{4\pi a_1^2 H_1}{C_h} \quad \text{and} \quad k_{c2} = \frac{4\pi a_2^2 H_2}{C_p}.$$

Here $C_p = \frac{4}{3}\pi(a_2^3 - a_1^3)c_1\rho_1$ is the heat capacity of the protein. For large values of time, the cooling still passes over to the thermal diffusion limit.

$$T_h = T_1 = T_2 = \frac{C_h}{8\rho_2 c_2(\pi\kappa_2 t)^{3/2}} + \cdots \qquad (21)$$

RESULTS AND DISCUSSION

For convenience, the normalized temperature, v, will be used in much of following discussion when $\langle\dot{Q}\rangle = 0$. The normalized temperature is defined as

$$v(t) = \frac{T(t) - T_0}{T^* - T_0} \qquad (22)$$

where T_0 is the initial solvent temperature and T^* is the initial temperature of the chromophore when the laser pulse terminates ($\langle\dot{Q}\rangle = 0$).

In Fig. 2 we display plots of the normalized chromophore temperature as function of time based on the one boundary model. The squares are the predictions of the model (Eq. 7), whereas the dashed lines show the exponential decay at short times (Eq. 8) and the solid lines give the diffusion limit at large time (Eq. 9). In panel *a*, we use water as a surrounding medium. The coefficient of surface heat transport, H, is estimated from the Raman analysis described previously (Li et al., 1992). The first two decades of thermal relaxation take place on the ps time scale, in agreement with the results of molecular dynamics simulations (Henry et al., 1986). However, because the thermal conductivity of the protein material is expected to be smaller than water (Anderson, 1981), we depict in panel *b*) the results when the thermal conductivity is reduced. Under this condition the diffusion limit becomes more important, and the exponential approximation begins to break down. Panel *c*) depicts the situation when H is also reduced so that the exponential decay again becomes a very good approximation over a large dynamic range.

Notice that the parameters ρ, c, a can be well approximated by independent experiments. For example, we can find the specific heat of the heme group by using explicit vibrational frequencies (Henry et al., 1986) $C_h(300K) = 0.82 \times 10^{-21}$ *J/K*], or by using values reported for bulk protein material (Mrevlishvili, 1979) [$C_h(300 - 400K) = 1.2 - 1.6 \times 10^{-21}$ *J/K*]. Here we take $C_h = 1 \times 10^{-21}$ *J/K*. The thermal conductivity K can also be measured by the technique of impulsive stimulated thermal scattering (Duggal et al, 1991 and 1992) in protein films or crystals. The coefficient of surface heat transport, H, has been estimated previously using anti-Stokes/Stokes Raman saturation data (Li et al., 1992).

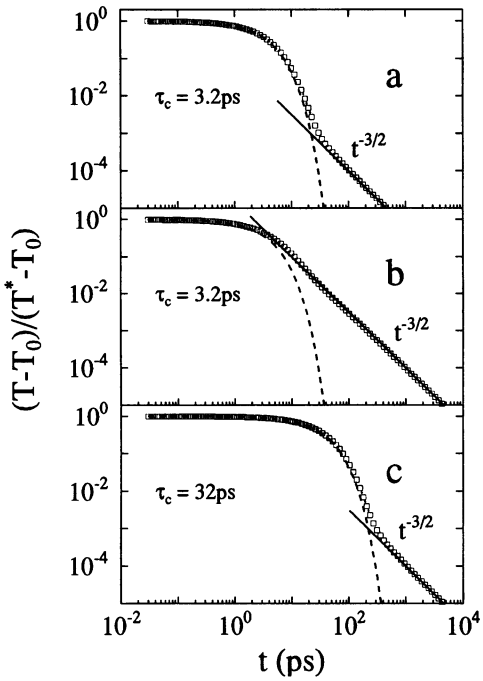

FIGURE 2 The plot of normalized heme temperature v_h vs. time for a simplified one boundary model. The square symbols are the predictions of Eq. 7 With a = 0.5 nm, $C_h = 1.0 \times 10^{-21}$ J/K, $c\rho = 4.18$ J/Kcm^3. In the top panel (*a*), $K = 6.0 \times 10^{-3}$ W/Kcm and $H = 1.0 \times 10^4$ W/Kcm^2; in the middle panel (*b*), $K = 6.0 \times 10^{-4}$ W/Kcm and $H = 1.0 \times 10^4$ W/Kcm^2; in the bottom panel (*c*), $K = 6.0 \times 10^{-4}$ W/Kcm and $H = 1.0 \times 10^3$ W/Kcm^2. The dashed lines are the short time approximations using Eq. 8 with $\tau_c = a/Dh\kappa = C_h/4\pi a2H$. The solid lines are the long time approximations using Eq. 9.

The predictions of the more realistic two boundary model are shown in Fig. 3 by the open squares. As an example of the two boundary model we use the heme chromophore surrounded by protein material, with water as the solvent. The thermal conductivity of the protein, K_1, is estimated by taking the average value from various protein materials (Anderson, 1981). The surface conductivities at each boundary (H_1 and H_2) are unknown but in principle can be found by comparisons to experiments that directly monitor the thermal decay, such as time resolved anti-Stokes/Stokes Raman scattering. In the upper panel of Fig. 3, we take the surface conductivity to be $H_1 = H_2 = 10^4$W/Kcm^2 as estimated previously from the simplified one boundary analysis (Li et al., 1992). The major part of the cooling still takes place in less than 10 ps. However, because the thermal conductivity of the protein, K_1, is less than water, the temperature in the two boundary model is maintained at a higher level between 1–100 ps than in the one boundary model. For reference, the dotted line in Fig. 3 *a* gives the results of the one boundary model from Fig. 2 *a*. The solid lines are the long time thermal diffusion approximations from Eq. 21, and the dashes are the short time double exponential approximations from Eq. 20. If we reduce the coefficient of heat transport at the boundary between the

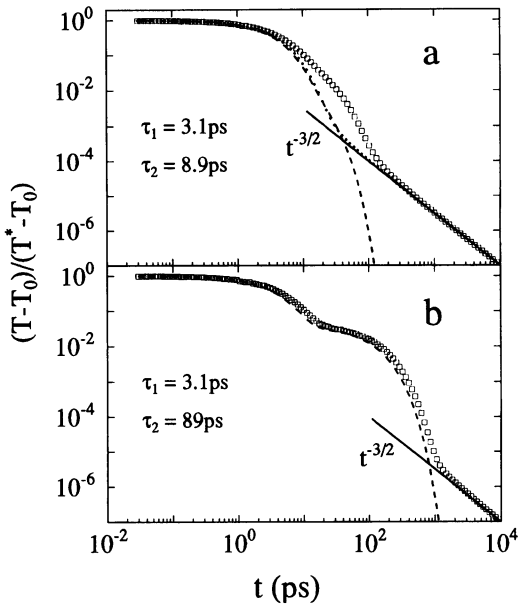

FIGURE 3 The plot of normalized heme temperature v_h vs. time for the two boundary model. The square symbols are the predictions of the two boundary model with $a_1 = 0.5$ nm, $a_2 = 1.5$ nm, $C_h = 1.0 \times 10^{-21}$ J/K, $c_1\rho_1 = 2.0$ J/Kcm^3, and $c_2\rho_2 = 4.18$ J/Kcm^3. For the upper panel (a), $K_1 = 1.0 \times 10^{-3}$ W/Kcm, $K_2 = 6.0 \times 10^{-3}$ W/Kcm, and $H_1 = H_2 = 1.0 \times 10^4$ W/Kcm^2; in the lower panel (b) all parameters are same as the upper one except $H_2 = 1.0 \times 10^3$ W/Kcm^2. The dotted line is the one boundary model result with $a = 0.5$nm, $c\rho = 4.18$ W/Kcm^3, $K = 6.0 \times 10^{-3}$ W/Kcm, and $H = 1.0 \times 10^4$ W/Kcm^2. The solid lines are long time approximations from Eq. 21 and the dashed lines are the short time approximations from Eq. 20.

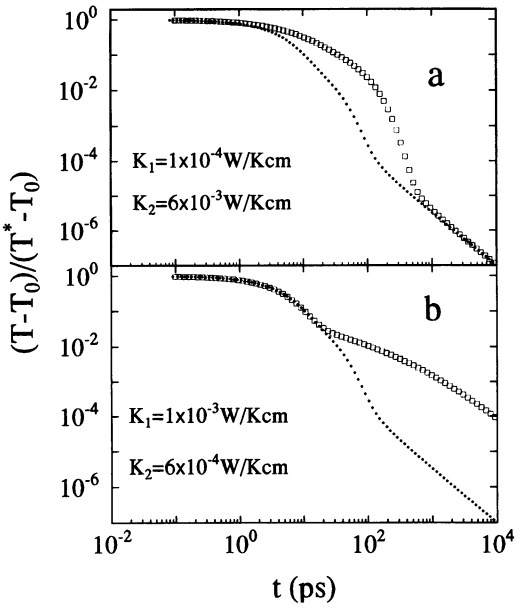

FIGURE 4 The plot of normalized temperature v_h vs. time using different conductivity for the protein and solvent with $H_1 = H_2 = 1.0 \times 10^4$ W/Kcm^2. The dotted lines are from Fig. 3 with $K_1 = 1.0 \times 10^{-3}$ W/Kcm and $K_2 = 6.0 \times 10^{-3}$ W/Kcm.

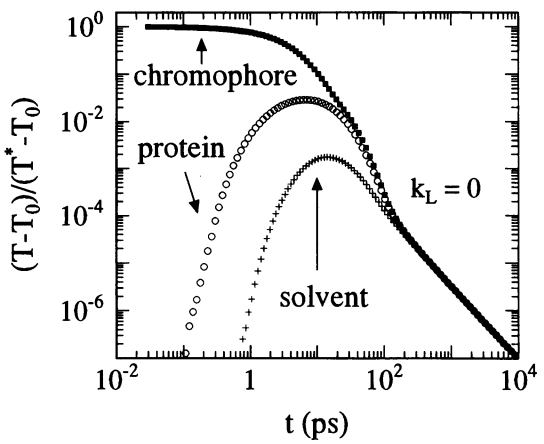

FIGURE 5 A plot of normalized temperatures as a function of time at different positions with $a_1 = 0.5$ nm, $a_2 = 1.5$ nm, $H_1 = H_2 = 1.0 \times 10^4$ W/Kcm^2, $K_1 = 1.0 \times 10^{-3}$ W/Kcm and $K_2 = 6.0 \times 10^{-3}$ W/Kcm. The solid squares are at r = 0, the circles are at r = 1.0 nm, and the crosses are at the solvent interface, $r = 1.5^+$ nm.

protein and solvent (H_2) by one order of magnitude, the double exponential nature of the decay is made even more evident (lower panel). The two time constants for the double exponential decay (given by k_1^{-1} and k_2^{-1} in Eq. 20) in the upper panel of Fig. 3 agree well with the previous molecular dynamics simulations (Henry et al., 1986).

As might be expected, the thermal conductivities K_1 and K_2 also play an important role in the heat transport. In Fig. 4 we demonstrate how reducing K_1 (*upper*) and K_2 (*lower*) by one order of magnitude affects the vibrational cooling dynamics. The dotted line is the simulation using the parameters of Fig. 3 *a*. As can be seen, reducing K_1 slows the cooling in the 1 ps to 1 ns range, and reducing K_2 slows the cooling at times longer than 10 ps.

From numerical calculations we can also get the temperature of the protein and solvent as a functions of position. Fig. 5 shows the cooling simulation ($\langle\dot{Q}\rangle = 0$) for the chromophore, protein and solvent using the two boundary model. Because the specific heat of the protein is 20 to 30 times larger than that of the chromophore, the highest temperature of the protein is only $\sim 5 \times 10^{-2}$ of $v_h(0)$. This corresponds to a $\sim 25K$ transient rise in temperature of the protein, assuming the chromophore vibrational temperature is increased by $500K$ upon absorption of a photon. All temperatures will converge and follow the same diffusion limit decay after $\sim$ 100 ps. Fig. 6 shows the spatial profile of the temperature at several times.

The process of laser heating can also be simulated and is shown in Fig. 7. Here we use an initial photoexcitation rate of $k_L = \tilde{J}\sigma_A \sim 4 \times 10^{11}$s^{-1}, which is typical for a focused 420-nm, 10-ns laser pulse being absorbed by a heme protein (average power of 15 mW at 100 Hz with $\tilde{J} \sim 10^{27}$ photon/sec – cm^2 for the photon flux and $\sigma_A \sim 4 \times 10^{-16}$cm^2 for the absorption cross-section). However, when we consider the ground state population loss because of saturation (Li et al., 1992), the average photoexcitation rate under photo-

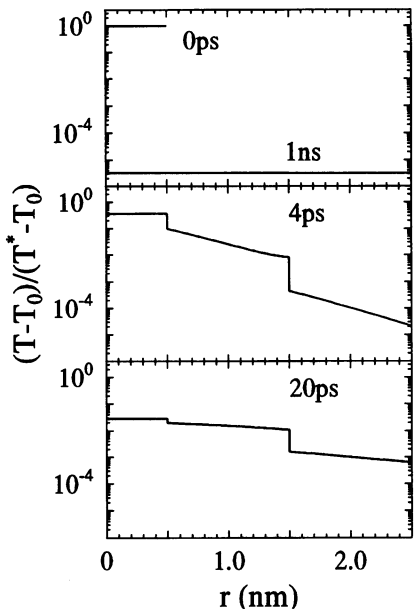

FIGURE 6 A plot of the normalized temperature as a function of position at different times. In panel (*a*) when $t = 0$, $v = 0$ for $r > a_1$, so it can not be shown in the figure. All parameters are the same as in Fig. 5.

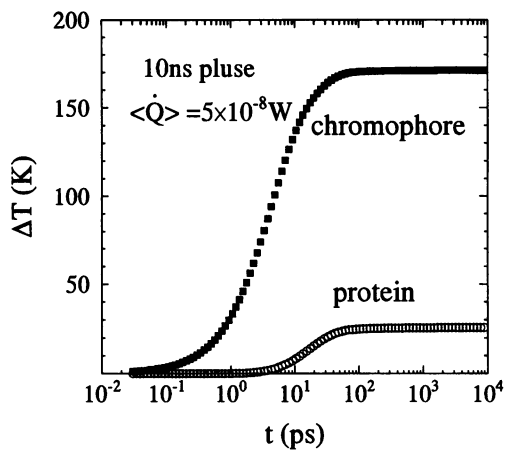

FIGURE 7 A plot of the temperatures of the chromophore and protein as a function of time during photon driven heating. All thermal parameters are the same as in Fig. 5 and $\langle \dot{Q} \rangle = 5 \times 10^{-8} W$. The protein temperature is evaluated at $r = 1.0$nm.

stationary conditions corresponds to a photon absorption every 8–9 ps (under saturation conditions, $\langle \dot{Q} \rangle \cong h\nu_L \tilde{J}\sigma_A/(1 + \tau\tilde{J}\sigma_A) \sim 5 \times 10^{-8} W$, with a ground electronic state recovery time (Li et al., 1992) for heme proteins of $\tau \sim 6$ps). This is on the order of the time constants for double exponential decay given in Fig. 3 *a* and leads to a steady-state protein temperature that is increased by only about 25*K* (e.g., see Fig. 7). Note that the temperature of the chromophore and the protein both saturate at ~100ps as photostationary state conditions are established. The steady-state temperature of the chromophore is increased by about 170*K* using the parameters in Fig. 3 *a*. This is very close to the value extracted from the anti-Stokes/Stokes measurements (Li et al., 1992).

SUMMARY

In this work, we have shown how a simple classical heat transport model can be used to describe the thermal response of photoexcited biomolecules. In this model, only a few parameters are needed, and most of them can be experimentally determined using independent measurements (Li et al., 1992).

We have shown how the temperatures of the chromophore, protein and solvent can be simulated as functions of time and position during photon-driven heating and cooling processes. The results show that the time scales of significant temperature change for both processes are in the ps range and indicate that the photoexcitation of a chromophore is likely to affect the biological transport rates if they occur on the ps time scale. For most cases of practical interest, the temperature of the chromophore appears as a double exponential decay in the short time limit. At longer times the thermal decay "rolls over" to a diffusion limit ($t^{-3/2}$). Figs. 2 and 3 demonstrate that the closed form expressions, Eqs. 8, 9, 20, and 21, provide a simple and useful approximation to the thermal response under most circumstances.

In a more precise treatment, the specific heats of the chromophore and the protein (assumed constant here) will be increasing functions of temperature (Mrevlishvili, 1979; Landau and Lifshitz, 1980). This leads to an additional effect, where the specific heat rises during laser heating and further slows the rate of chromophore cooling (see Eqs. 8 and 20). One can imagine that a positive feedback mechanism of this type could be utilized in natural photon driven biological processes (e.g., photosynthesis, vision) to irreversibly enhance certain key transport rates (e.g., energy migration, isomerization, or charge separation).

The simple thermal transport model presented here shows good agreement with the results of molecular dynamics simulations (Henry et al., 1986). From a practical point of view, use of such a model facilitates the interface between experiments, which are able to extract only a few parameters, and the more sophisticated molecular dynamics simulations, which depend upon many degrees of freedom with unknown interaction strengths. Most importantly, the results presented here show that transient thermal effects cannot be neglected when monitoring kinetic events in biomolecules on the ps time scale.

APPENDIX

In general, the inverse Laplace transform is given by

$$F(t) = \frac{1}{2\pi i} \int_{\gamma - i\infty}^{\gamma + i\infty} \bar{F}(p) e^{pt}\, dp. \qquad \text{(A1)}$$

where γ is so large that all the singularities of $\bar{F}(p)$ lie to the left of the line $(\gamma - i\infty, \gamma + \infty)$.

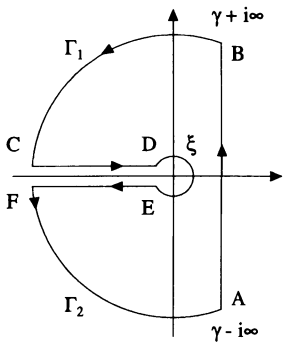

FIGURE A1 The contour used to evaluate the integral in Eq. A.2.

Using the contour shown in Fig. 1 *A*, we have

$$\int_A^B + \int_{\Gamma_1} + \int_C^D + \int_\xi + \int_E^F + \int_{\Gamma_2} = 2\pi i \Sigma \mathrm{Res} \qquad \text{(A2)}$$

In our problem $\bar{F}(p)=\bar{v}(\sqrt{p})$, and there is no singularity for $\bar{v}(\sqrt{p})$, inside the contour, so $\Sigma\mathrm{Res} = 0$. Let $p = \rho e^{i\phi}$, when $\rho \to \infty$, $\int_{\Gamma_1} = \int_{\Gamma_2} = 0$. So we get

$$\int_{\gamma - i\infty}^{\gamma + i\infty} = \int_A^B = -\int_C^D - \int_E^F - \int_\xi \quad (R \to \infty) \qquad \text{(A3)}$$

For the path $C \to D$, $p = \rho e^{i\pi}$; for the path $E \to p$, $p = \rho e^{-i\pi}$; for the path ξ, $p = \epsilon e^{i\phi}$ and we let $\epsilon \to 0$ to find

$$\int_C^D \bar{v}(\sqrt{p}) e^{pt}\, dp = -\int_\infty^0 \bar{v}(i\sqrt{\rho}) e^{-\rho t}\, d\rho$$

$$= \int_0^\infty \bar{v}(i\sqrt{\rho}) e^{-\rho t}\, d\rho;$$

$$\int_E^F \bar{v}(\sqrt{p}) = -\int_0^\infty \bar{v}(-i\sqrt{p}) e^{\rho t}\, d\rho.$$

So

$$-\int_C^D - \int_E^F = \int_0^\infty [\bar{v}(-i\sqrt{\rho}) - \bar{v}(i\sqrt{\rho})] e^{-\rho t}\, dp. \qquad \text{(A4)}$$

Let $\bar{v}(\sqrt{p}) = g(p)/p$, and $P = \epsilon e^{i\phi}$, then

$$\int_\xi \bar{v}(\sqrt{p}) e^{pt}\, dp = i \int_\pi^{-\pi} g(\sqrt{\epsilon} e^{i\phi/2}) e^{-\epsilon t e^{i\phi}}\, d\phi.$$

When $\epsilon \to 0$,

$$\int_\xi \bar{v}(\sqrt{p}) e^{pt}\, dp = -2\pi i g(0), \qquad \text{(A5)}$$

Changing ρ back to p, and notice that $\bar{v}(\sqrt{p})$ *and* $v(t)$ are real functions, we can get

$$\begin{aligned} v(t) &= -\int_\xi - \int_C^D - \int_E^F \\ &= g(0) + \frac{1}{\pi} \int_0^\infty \mathrm{Im}[\bar{v}(-i\sqrt{p})] e^{-pt}\, dp. \end{aligned} \qquad \text{(A6)}$$

This work was supported by NSF 90–16860 and NIH AM 35090.

REFERENCES

Anderson, H. L. 1981. AIP 50th Anniversary Physics Vade Mecum. American Institute of Physics, New York. 50 pp.

Brack, T. L., and G. H. Atkinson. 1991. Vibrationally excited retinal in the bacteriorhodopsin photocycle: picosecond time-resolved anti-Stokes resonance Raman scattering. *J. Phys. Chem.* 95:2351–2356.

Carslaw, H. S., and J. C. Jaeger. 1959. Conduction of Heat in Solids. Oxford University Press, Oxford. 349–350.

Duggal, A. R., and K. A Nelson. 1991. Picosecond-microsecond structural relaxation dynamics in polypropylene glycol: impulsive stimulated light-scattering experiments. *J. Chem. Phys.* 94:7677–7688.

Duggal, A. R., J. A. Rogers, and K. A. Nelson. 1992. Real-time optical characterization of surface acoustic modes of polyimide thin-film coatings. *J. Appl. Phys.* 72:2823–2839.

Henry, E. R., W. A. Eaton, and R. M. Hochstrasser. 1986. Molecular dynamics simulations of cooling in laser-excited heme proteins. *Proc. Natl. Acad. USA.* 83:8982–8986.

Kesavamoorthy, R., M. S. Super, and S. A. Asher. 1992. Nanosecond photothermal dynamics in colloidal suspension. *J. Appl. Phys.* 71:1116–1123.

Landau, L. D., and E. M. Lifshitz. 1980. Statistical Physics. Pergamon Press Ltd, New York. 158–190.

Li, P., J. T. Sage, and P. M. Champion. 1992. Probing picosecond processes with nanosecond lasers: electronic and vibrational relaxation dynamics of heme proteins. *J. Chem. Phys.* 97:3214–3227.

Lingle, R., X. Xu, H. Zhu, S. Yu, and J. B. Hopkins. 1991a. Direct observation of hot vibrations in photoexcited deoxyhemoglobin using picosecond Raman spectroscopy. *J. Am. Chem. Soc.* 113:3992–3994.

Lingle, R., X. Xu, H. Zhu, S. Yu, and J. B. Hopkins. 1991b. Picosecond Raman study of energy flow in a photoexcited heme protein. *J. Chem. Phys.* 95:9320–9331.

Miller, R. J. Dwayne. 1991. Vibrational energy relaxation and structural dynamics of heme protein. *Annu. Rev. Phys. Chem.* 42:581–614.

Mrevlishvili, G. M. 1979. Low temperature calorimetry of biological macromolecules. *Sov. Phys. Usp.* 22:433–455.

Schomacker, K. T., and P. M. Champion. 1986. Investigations of spectral broadening mechanisms in biomolecules: cytochrome-c. *J. Chem. Phys.* 84:5314–5325.